AD-A122 339 RAIN CLUTTER STATISTICS(U) NAVAL RESEARCH LAB 1/1
WASHINGTON DC W B GORDON ET AL. 30 SEP 82 NRL-8639
SBI-AD-E000 513

UNCLASSIFIED F/G 17/9 NL

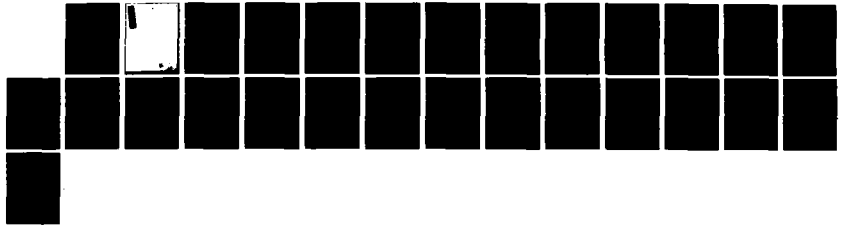

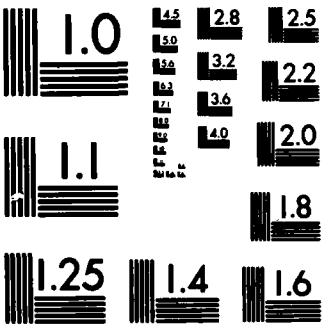

MICROCOPY RESOLUTION TEST CHART
NATIONAL BUREAU OF STANDARDS-1963-A

AD A122339

SECURITY CLASSIFICATION OF THIS PAGE (When Data Entered)

REPORT DOCUMENTATION PAGE		READ INSTRUCTIONS BEFORE COMPLETING FORM
1. REPORT NUMBER NRL Report 8639	2. GOVT ACCESSION NO. AD A12233	3. RECIPIENT'S CATALOG NUMBER 9
4. TITLE (and Subtitle) RAIN CLUTTER STATISTICS		5. TYPE OF REPORT & PERIOD COVERED Interim report on a continuing NRL Problem. 6. PERFORMING ORG. REPORT NUMBER
7. AUTHOR(s) William B. Gordon and Jon D. Wilson		8. CONTRACT OR GRANT NUMBER(s)
9. PERFORMING ORGANIZATION NAME AND ADDRESS Naval Research Laboratory Washington, DC 20735		10. PROGRAM ELEMENT, PROJECT, TASK AREA & WORK UNIT NUMBERS 61153N RR0210541 NRL Problem 53-0628-0
11. CONTROLLING OFFICE NAME AND ADDRESS Office of Naval Research Arlington, VA 22217		12. REPORT DATE September 30, 1982 13. NUMBER OF PAGES 25
14. MONITORING AGENCY NAME & ADDRESS(if different from Controlling Office)		15. SECURITY CLASS. (of this report) Unclassified 15a. DECLASSIFICATION/DOWNGRADING SCHEDULE

16. DISTRIBUTION STATEMENT (of this Report)

Approved for public release; distribution unlimited.

17. DISTRIBUTION STATEMENT (of the abstract entered in Block 20, if different from Report)

18. SUPPLEMENTARY NOTES

19. KEY WORDS (Continue on reverse side if necessary and identify by block number)

Rain clutter
Radar design
Doppler spectrum
Power-versus-frequency law

20. ABSTRACT (Continue on reverse side if necessary and identify by block number)

Measurements of rain clutter were taken with a frequency-agile S-band radar for the purpose of studying the Doppler power spectra and the variation of backscattered power with space, time, and frequency. The clutter was found to be nonhomogeneously distributed in both space and time, but the relation of mean backscattered power to frequency seemed to involve only a single parameter having a spatial and temporal variation. Although the radar was looking into the surface wind, a significant portion of the backscattered signal energy was always found to lie

(Continued)

DD FORM 1 JAN 73 1473 EDITION OF 1 NOV 65 IS OBSOLETE
S/N 0102-014-6601

SECURITY CLASSIFICATION OF THIS PAGE (When Data Entered)

20. ABSTRACT (Continued)

in the negative frequency range, suggesting a wind shear, estimated to be about 8 m/s per km. The Doppler power spectra were sometimes found to have multiple peaks at both positive and negative Doppler frequencies, and from measurements of the peak widths it appears that they were produced by horizontal bands or clumps of clutter whose vertical extent was of the order of 200 m. Another possibility for the production of multiple spectral peaks is Bragg scattering from turbulent eddies. However, using statistical methods which are valid in the presence of calibration errors and noise, it was established that the data favored the vertical-stratification mode over the Bragg-scattering model. The nonhomogeneity of the clutter and the existence of Doppler spectra with multiple peaks have serious implications for the performance and design of detectors.

CONTENTS

DTIC COPY INSPECTED 2

Accession For
NTIS GRA&I ☑
DTIC TAB ☐
Unannounced ☐
Justification
By
Distribution/
Availability Codes
Dist | Avail and/or Special
A

RAIN CLUTTER STATISTICS

INTRODUCTION

The rain clutter data presented in this report were taken with a frequency-agile *S*-band radar whose parameters are shown in Table 1. Five equispaced frequencies from 2.1 to 3.9 GHz were transmitted and were varied from pulse to pulse such that every fifth pulse had the same frequency. With this radar a single antenna is used for both transmission and reception over the entire range of frequencies. The data were taken on 5 September 1979 at the Randle Cliff facility of the Naval Research Laboratory during the remnants of hurricane David. The wind at the surface was from the northeast at approximately 23 knots. The facility is on the western shore of the Chesapeake Bay, and the radar coverage lay in the northeast quadrant, with the radar looking over the Bay and into the wind.

Table 1 — Radar Parameters

Frequencies:	2.1, 2.55, 3.0, 3.45, and 3.9 GHz, varied from pulse to pulse
PRF:	1600/s
Beamwidth:	1° in azimuth and 2° in elevation (at 3.0 GHz)
Pulse width:	compressed to 0.7 μs
Antenna rotation:	0, 2, and 6 RPM
Polarization:	vertical

Our main concerns were the functional relationship between the mean backscattered power and frequency, the spatial and temporal variation of the backscattered signal, and the Doppler power spectra. Among our results, those concerned with the clutter Doppler spectra have the greatest potential importance for the radar engineer, since it is the properties of these spectra which determine the effectiveness of clutter-rejection filters. A Gaussian model for rain clutter spectra is generally accepted by the radar community (as in Ref. 1, for example), and the early experimental works of Barlow [2] and Kerr [3] are still cited as primary sources on this subject. However, we found that the Doppler spectra sometimes had multiple peaks, and we would like to learn something about the nature of the processes which can produce such multipeaked spectra and how frequently they can occur. The simplest explanation for the occurrence of such spectra is that of a wind shear operating on a vertically stratified distribution of clutter, but there are other possibilities. One such possibility frequently discussed in the literature is that of Bragg scattering from turbulent eddies, but the variation of backscattered power with space, time, and frequency that we observed is more consistent with the vertical-stratification model.

From the spatial and temporal variation of certain statistics we found that the observed relationship between the mean backscattered power and frequency conformed to the model $P(f) = AQ(f)$, where $Q = Q(f)$ is some function which depends *only* on frequency and A is a frequency-independent parameter which varies with time and position. For the Bragg-type scattering effects discussed in the literature we have $Q(f) = f^n$, where the exponent n has a value between 0 and 2. But from the data we conclude that the exponential rate of growth of power with frequency lies in the range $3 < n < 7$, with the preferred value being approximately $n = 5$, which happens to be the value of n which

Manuscript submitted August 13, 1982.

corresponds to incoherent scattering from narrow horizontal bands. This analysis is complicated by the possible existence of calibration errors whose effects cannot be averaged out, because they are constant and multiplicative. For this reason (as well as others) we did *not* estimate the value of n by fitting a curve to the data in the usual sense of least-squares regression. Instead we calculated the smallest RMS calibration error that would be required to produce the departure of measured values of n from an assumed "true" value. We judge that the RMS calibration error was no larger than 2 dB (except for a glitch at the highest frequency, to be described in the section on system calibration); hence values of n lying in the range $0 \leqslant n \leqslant 2$ are rejected as reasonable possibilities, because they would imply an RMS calibration error greater than 3 dB.

A final remark concerning methodology: The performance of radars is determined by the state of the clutter at particular times and particular places. Thus our interest is in the behavior of the rain backscatter over short intervals of time and localized regions of space. We are not very interested in establishing trends in data which are heavily averaged over space and time, and stationarity was assumed only for data originating from a single range cell over a short duration of time.

ORGANIZATION OF THE DATA

The basic data from the radar consists of A/D converted *I*- and *Q*-channel voltages, which are organized into data records, each consisting of 28,130 16-bit words. These data records are temporarily stored in a minicomputer before being dumped onto tape. Each radar pulse gives rise to a block of data consisting of two 16-bit words recording the carrier frequency and azimuth and M_c 16-bit words recording the *I*- and *Q*-channel voltages, with eight bits being assigned to each channel, where M_c is a variable indicating the total number of range cells per pulse being processed. Hence, the total number of pulses N_p in a record is

$$N_p = \frac{28,130}{2 + M_c}.$$

The data are sampled at a rate of 3 MHz, which is twice the reciprocal of the compressed pulse width of 0.7 μs. Hence there is a 50% overlap between successive range cells.

When the antenna is rotating, the recording device is triggered to take data centered at a given azimuth. Thus, for example, there is a 10-s delay between records when the antenna is rotating at 6 RPM. When the antenna is not rotating, there is approximately a 2-s delay between records.

The data records are either single-frequency or multifrequency records. The single-frequency records always use the carrier frequency of 3.0 GHz, whereas the multifrequency records use each of the five frequencies given in Table 1. In the multifrequency case the frequencies are varied in order from pulse to pulse; hence the PRF for pulses at each given frequency is reduced from 1600 to 320 in the multifrequency case.

Finally, for convenience the data records are grouped into files, with each file consisting of records taken at a given azimuth and centered at a given range. In effect a file consists of data from a selected clutter cell appearing on the PPI scope. Table 2 gives the file descriptions for the files referred to in this report. Of special interest is file 8, which was obtained by turning off the transmitter. This file will be referred to as the noise file and is used to measure the receiver noise statistics. File 3 is the only single-frequency file used in this report. Figure 1 shows a schematic PPI display of the regions covered by the four multifrequency files: 1, 2, 5 and 6.

Table 2 — File Descriptions

File No.	General Description	Antenna (RPM) Rate	Range (km)	Az. (deg)	El. (deg)	No. of Records	Time Duration per Record (s)	No. of Range Cells
1	Multifrequency	6	18.95	359	3.6	10	0.27	64
2	Multifrequency	6	29.20	57	3.6	10	0.27	64
3	Single Frequency	6	29.20	57	3.6	5	0.27	64
5	Multifrequency	2	31.78	354	3.2	5	1.76	8
6	Multifrequency	0	33.34	40	3.2	10	1.76	8
8	Multifrequency noise	—	—	—	—	5	0.52	32

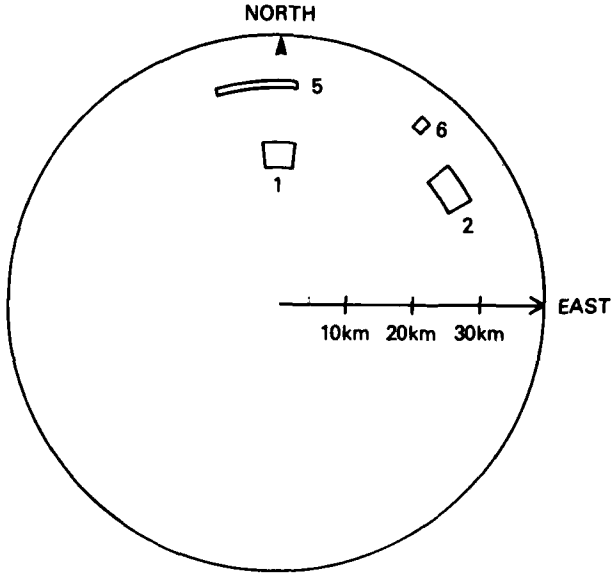

Fig. 1 — Coverage areas for files 1, 2, 5, and 6

VOLTAGE AND POWER HISTOGRAMS

Let x_n and y_n denote the I- and Q-channel voltages measured at a given range from the nth pulse at a given frequency. From general principles one would expect x_n and y_n to behave like uncorrelated zero-mean Gaussian variables with the same variance:

$$E[x_n] = E[y_n] = 0,$$

$$E[x_n^2] = E[y_n^2] = \sigma^2,$$

$$E[x_m y_n] = 0.$$

Figure 2 shows histograms of the I- and Q-channel voltages as they actually come off the A/D converter. Due to a fault in the A/D conversion, there are no -1s and 0s in the I channel, and the 0s and 1s are underrepresented in the Q channel. The main effect of those malfunctions in the low-order bits appears to be the production of small systematic biases. These biases do not seem to vary much from file to file (even including the noise file), but they do vary slightly with frequency. These biases are removed numerically, and the data thus obtained are said to be bias corrected.

Table 3 shows values of the crosscorrelation between the bias-corrected I- and Q-channel voltages. The values shown are averages obtained from all range cells in a given record, at each of the two indicated files. These correlation coefficients are small in magnitude and negative in sign, but they are

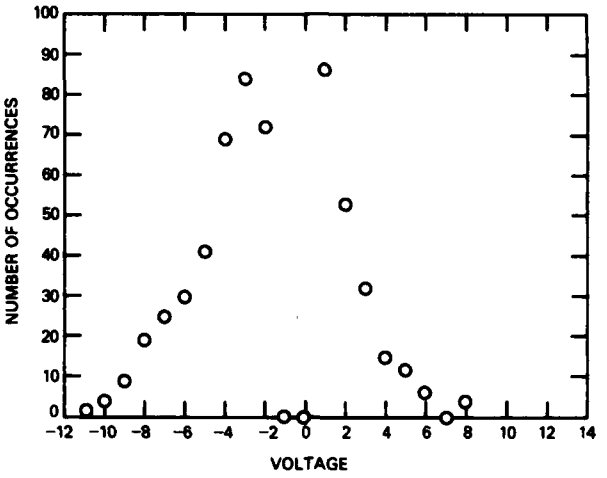

(a) *I*-channel voltage

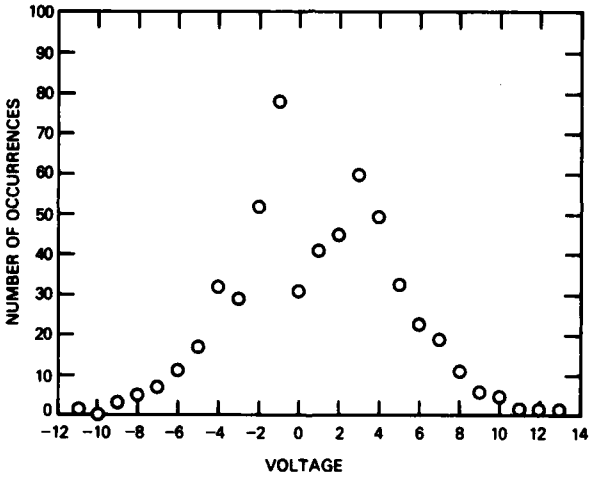

(b) *Q*-channel voltage

Fig. 2 — Voltage histograms: data from file 6 at 3.9 GHz

Table 3 — Crosscorrelation Between I- and Q-Channel Voltages

File	Crosscorrelation Coefficient				
	2.1 GHz	2.55 GHz	3.0 GHz	3.45 GHz	3.9 GHz
6	−0.0594	−0.0916	−0.0519	−0.0622	−0.0604
8	−0.0169	−0.0353	−0.0320	−0.0323	−0.0465

larger in magnitude when signal is present (the coefficients being larger for file 6 than for file 8, the noise file).

The bias-corrected data were used to generate histograms of instantaneous power, and these are shown in Fig. 3. Also shown, above each histogram, is a plot of the logarithms (base e) of the number of samples in each class interval. These plots provide a check of the validity of the Gaussian model as follows. The data are from multifrequency files, and since only every fifth pulse has a given frequency, the correlation between successive pulses at a given frequency is small. Hence the values of instantaneous power for each pulse at a given frequency should be independent samples of a variable $w = x^2 + y^2$, where x and y are two independent zero-mean Gaussian variables with variances both equal to σ^2. The variable w has the probability density q given by

$$q(w) = (1/w_0)e^{-w/w_0}, \tag{1}$$

where

$$w_0 = E[w] = 2\sigma^2.$$

The expected number ν of samples which fall in a class interval of length Δ centered at w is approximately

$$\nu = N\Delta q(w),$$

where N is the total number of samples. Hence $\ln \nu$ should be approximately linear in w:

$$\ln \nu = -(w/w_0) + \ln(N\Delta/w_0).$$

The straight lines shown in these plots are generated by this relation, with w_0 being taken to be the sample mean of the power. As can be seen, the fit is good.

SYSTEM CALIBRATION

For each of the five frequencies used, measurements were made of the antenna gain, receiver gain, transmitted power, and cable losses. These measurements were used to obtain "calibration factors" k_i ($i = 1, 2, 3, 4, 5$) which are proportional to the reciprocals of the total system response at each frequency. Calibrated values of power were obtained by multiplying the raw values by the factors k_i. These "calibrated" values are given in terms of unspecified units of power, since no attempt was made to measure the power in watts. Unfortunately we were not able to use a test sphere in the calibration.

Previous measurements had shown that the transmitter signal-to-noise power ratios were 38 dB or better over the entire frequency range. Hence the transmitter noise was not an important factor in our data analysis, since the corresponding receiver noise levels were orders of magnitude larger.

Examples of the calibrated power as a function of frequency are shown in Table 4 and Fig. 4. The table shows the sample mean and standard deviation for each of the indicated range cells from the same indicated record. Also shown is the number of pulses per frequency. The power is calculated from the bias-corrected data, and the corresponding means and standard deviations are essentially equal, as would be expected if the observed values of instantaneous power were random samples from the exponential distribution (Eq. (1)).

The power-versus-frequency curve shown in Fig. 4 was obtained by averaging all the data in file 6; however, the curves obtained from data in any individual record from any individual range cell all have the same general appearance. In particular, there is always a sharp drop off in power at the highest frequency, 3.9 GHz. A spectrum analyzer was used in an attempt to discover malfunctions in the signal synthesizer or transmitter at this frequency, but none was detected. Therefore we provisionally ascribe this anomally to an unidentified calibration error. As will be seen, the existence of this anomaly has no effect on our conclusions; in particular, the returns from the first four frequencies were sufficient to exclude Bragg scattering as a significant factor in the production of the Doppler spectral peaks.

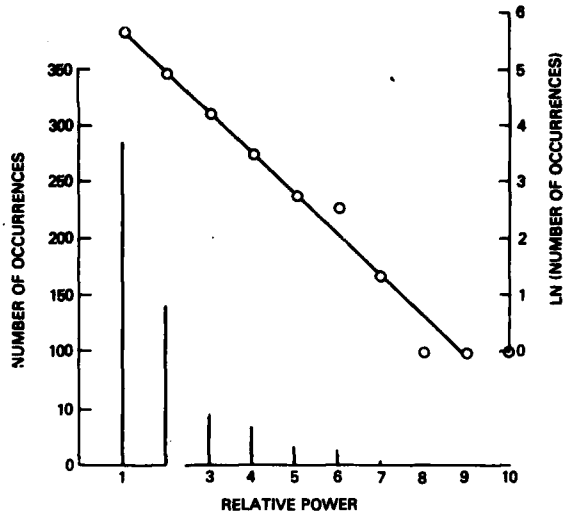

(a) 2.1 GHz

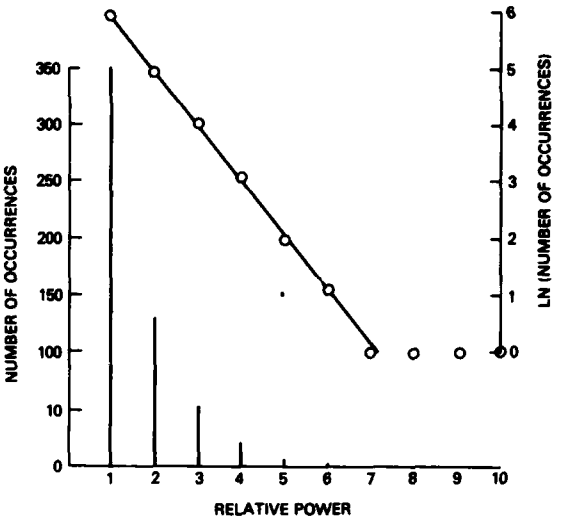

(b) 2.55 GHz

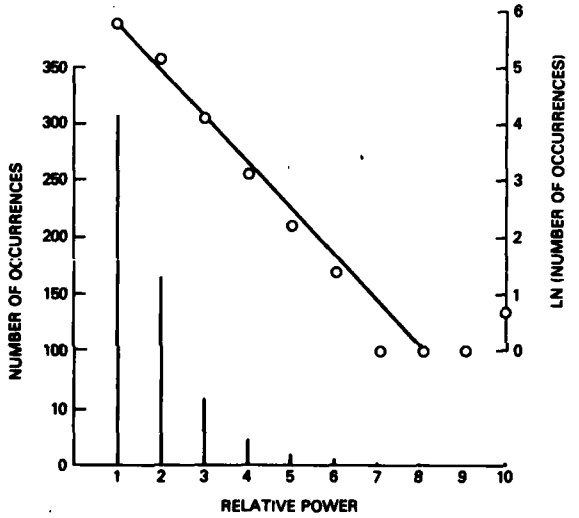

(c) 3.0 GHz

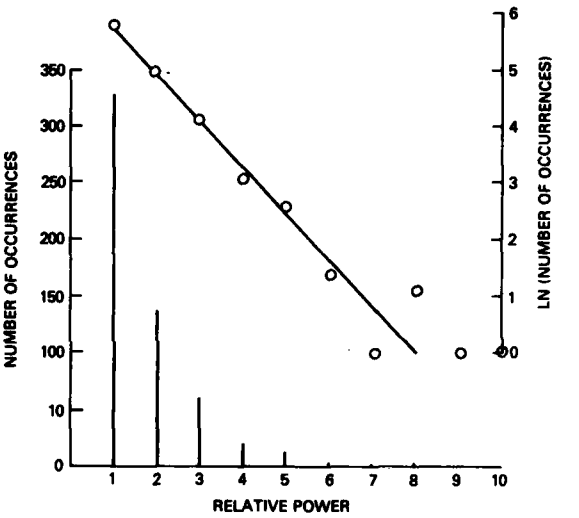

(d) 3.45 GHz

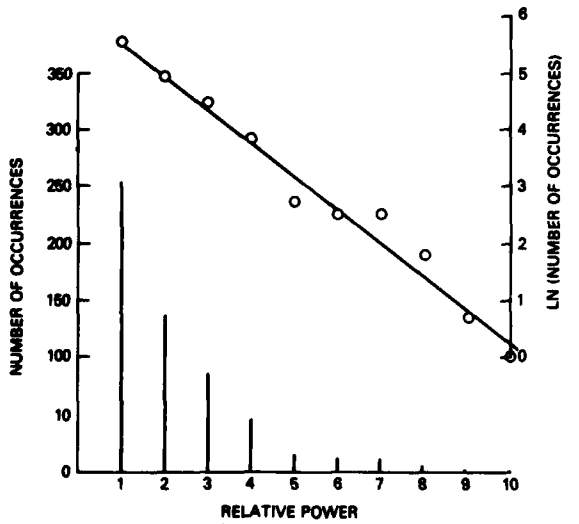

(e) 3.9 GHz

Fig. 3 — Power histograms and (upper plots) their logarithmic linearities

Table 4 — Mean and Standard-Deviation Values of Power for the Record-1 Data From File 6.

Frequency (GHz)	No. of Pulses	Mean	Std. Dev.
Range Cell 1			
2.1	561	35.2	34.6
2.55	561	104.4	100.2
3.0	561	214.7	211.4
3.45	561	317.0	323.7
3.9	562	186.3	182.4
Range Cell 2			
2.1	561	31.8	33.3
2.55	561	97.1	94.1
3.0	561	214.1	215.0
3.45	561	284.8	282.8
3.9	562	167.2	160.3
Range Cell 3			
2.1	561	29.3	28.6
2.55	561	96.2	95.2
3.0	561	210.5	203.8
3.45	561	274.5	268.7
3.9	562	176.8	164.1
Range Cell 4			
2.1	561	28.2	27.0
2.55	561	91.0	85.8
3.0	561	194.8	206.8
3.45	561	263.1	253.7
3.9	562	176.9	155.9

Frequency (GHz)	No. of Pulses	Mean	Std. Dev.
Range Cell 5			
2.1	561	28.7	27.9
2.55	561	8[illegible]7	80.8
3.0	561	170.6	176.6
3.45	561	253.4	259.1
3.9	562	172.6	171.9
Range Cell 6			
2.1	561	32.4	31.1
2.55	561	89.3	88.2
3.0	561	159.5	154.1
3.45	561	255.1	254.3
3.9	562	180.2	182.9
Range Cell 7			
2.1	561	33.0	30.7
2.55	561	88.5	93.4
3.0	561	179.6	188.1
3.45	561	264.6	249.3
3.9	562	178.0	170.4
Range Cell 8			
2.1	561	30.7	28.3
2.55	561	91.6	90.7
3.0	561	199.3	202.7
3.45	561	309.1	275.7
3.9	562	188.0	184.9

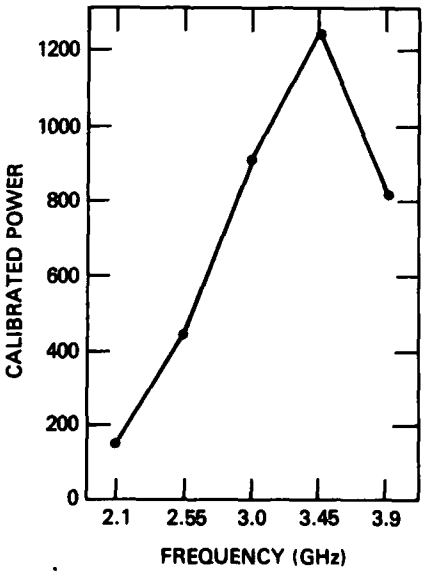

Fig. 4 — Calibrated power as a function of frequency for the data in file 6

DOPPLER POWER SPECTRA

Figures 5 and 6 show Doppler spectra from the first five consecutive records from the third range cell in multifrequency file 6, which is the only file with the antenna not rotating. As stated earlier, there is a 2-s delay between consecutive records in file 6. The PRF for pulses at a given frequency is 320 (=1600/5); hence the Nyquist interval is ±160 Hz and, for reasons to be explained, the Doppler resolution is 10 Hz. The spectra shown in Fig. 5 and 6 were taken from the backscattered return at 2.1 and 3.0 GHz, respectively. The relation between Doppler frequency δ and velocity v is $\delta = 2v/\lambda$. At 2.1 GHz, 1 Hz = 0.1388 knot, and at 3.0 GHz, 1 Hz = 0.0972 knot. Hence the Doppler resolution of 10 Hz is approximately 1.4 knots at 2.1 GHz and 1.0 knot at 3.0 GHz.

The Doppler power spectra are computed according to

$$I(\nu) = \frac{1}{N}\left|\sum_{n=0}^{N-1} z(nt)\, e^{-2\pi i \nu n t}\right|^2, \tag{2}$$

where N is the number of pulses used in the calculation, $z(t) = x(t) + iy(t)$ is the complex data formed from the I- and Q-channel voltages $x(t)$ and $y(t)$, and t is the interpulse period (=3.1 ms). Figures 5 and 6 show smoothed spectra for each of five records from the third range cell. The smoothing is accomplished by decomposing each record into a number M of smaller subrecords containing N pulses each, where N is a power of 2, and averaging the M "periodograms" (Eq. (2)) to obtain the spectra shown in the figures. In Figs. 5 and 6, $M = 17$ and $N = 32$, and the Doppler resolution is therefore 10 Hz. In each case the $I(\nu)$ are computed at increments of ν equal to the resolution. For graphical display the maximum value of $I(\nu)$ is normalized to unity.

When $x(t)$ and $y(t)$ are two stationary Gaussian zero-mean processes having the same autocorrelation function and zero crosscorrelation, then, by expanding the right-hand side of Eq. (2), one can easily establish that $I(\nu)$ has the form $U^2 + V^2$, where U and V are two zero-mean Gaussian variables which satisfy

$$E[U^2] = E[V^2],\ E[UV] = 0.$$

Hence for each value of ν the variable $w = I(\nu)$ has the exponential probability density function given by Eq. (1), and in particular its mean and standard deviation are equal. When the spectra are averaged as described, the mean remains the same but the standard deviation is reduced by the factor $1/\sqrt{M}$, where again M is the number of subrecords into which the original record has been divided. The averaging process therefore reduces the levels and numbers of spurious spectra peaks but at the cost of reduced resolution. These considerations suggest that some of the spectra shown in Fig. 5 are truly multimodal; that is, at least some of the peaks off the main lobe are physically real and not the spurious effects of random fluctuations. The width of these peaks, when they occur, is generally about 20 Hz, or 3 knots.

The existence of multiple peaks is less apparent in the return at 3.0 GHz, and all of the spikiness in Fig. 6 can be reasonably attributed to purely random fluctuations. In fact most of the spectra computed from the 3.0-GHz return was even more clearly "unimodal" than those shown in Fig. 6. The "most typical" spectrum at 3.0 GHz is shown schematically in Fig. 7 (which was obtained by averaging the spectra from the first five records from the sixth range cell). The hump appearing in the negative frequency range is significant; for although the radar was looking into the wind, in every spectrum that was examined (at either frequency) a significant portion of the backscattered signal energy lies in the negative frequency range.

The wind shear can be crudely estimated by supposing the wind-velocity null to occur somewhere between the upper and lower 3-dB points of the radar beam. For the 3.0-GHz beam at the range and elevation angle indicated for file 6 in Table 2, these two points occur at the heights 1.28 and 2.44 km.

Therefore, given that the surface wind speed was 23 knots = 12.4 m/s, the wind shear was between 5 and 10 m/s per km. The extent of the radar beam between the first upper and lower *nulls* is approximately double that between the two 3-dB points, and, in particular, the lower null of the 2.1-GHz beam lay just above the surface. It thus appears that the vertical coverage of the beams contained rain falling near the surface and extended well into the cloud above.

The estimated value of wind shear can also be used to gauge the vertical extent Δh of the clutter producing a spectral peak whose velocity spread is Δv: $\Delta h = \Delta$v/shear. For the narrow 3-knot peaks discussed, Δh = 160 or 320 m for the wind-shear values of 5 or 10 m/s per km.

The five spectra shown in Fig. 8 were obtained from synthetically generated Gaussian data with a Gaussian spectrum and are presented here for comparison with the spectra shown in Figs. 5 and 6. Each of these spectra is again an average of 17 32-point periodograms, and, as previously mentioned, at each frequency such spectra have a standard deviation equal to the true spectral value divided by $\sqrt{17}$. The three Gaussian curves shown in each plot in Fig. 8 are: the "true" spectrum, the true spectrum plus one standard deviation unit, and the true spectrum minus one standard deviation unit. There turns out to be a 15% probability that the estimated spectrum will exceed the true value by at least one such unit and also, coincidently, an almost equal probability that the estimated spectrum will fall below the true value by at least the same amount. It can therefore be expected that 70% of the estimated spectral values will fall between the upper and lower curves shown in Fig. 8. The estimated spectra are as spikey as expected, but their underlying Gaussian character can be discerned.

Figure 9 shows two spectra taken from file 3, the single-frequency file. Both spectra are computed from the same set of data, but the first is the average of six 64-point periodograms, whereas the second is the average of 13 32-point periodograms. The Doppler resolutions are respectively 25 Hz (=2.5 knots) and 50 Hz (=5 knots), and the Nyquist interval has been expanded to $\pm$800 Hz, since the single frequency is transmitted at a PRF of 1600. In all of the spectra from this file, almost all the signal energy is in the frequency interval between $\pm$200 Hz, which increases our confidence that there is no appreciable spectral foldover in the spectra shown in Fig. 5, at a lower carrier frequency. Due to antenna rotation, each of the M subrecords into which the total record is divided originates from a different circular arc in space. (Counting the beamwidth, each of these arcs is about 2° wide, which at a range of 30 km amounts to 1 km.) Therefore, the averaging process will tend to smooth out features which vary with azimuth. The narrowness of the central peak is a striking feature that appears in many of the spectra from this file, again indicating that a large fraction of the total clutter return originates from clumps or horizontal bands whose vertical extent is rather small.

TEMPORAL AND SPATIAL AUTOCORRELATION

The power spectrum and autocovariance of a stationary process are a Fourier-transform pair. However, the temporal autocorrelation functions $\rho(m)$ plotted in Figs. 10 and 11 are computed directly from the data according to the formula

$$\rho(mt) = R_m/R_0,$$

where

$$R_m = \frac{1}{N-m} \sum_{n=0}^{N-m} x[nt] \cdot x[(n+m)t] \tag{3}$$

and, as before, $x(t)$ is the I-channel voltage. The autocorrelation of the complex process $z(t) = x(t) + iy(t)$ should be the same, on the assumption that the I- and Q-channel voltages are two independent processes with the same second-order statistics.

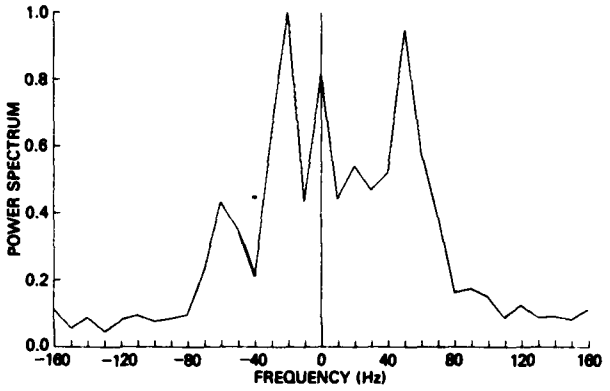

(a) Record 1

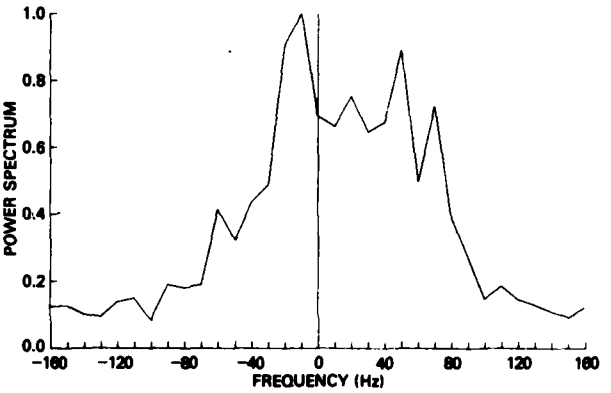

(b) Record 2

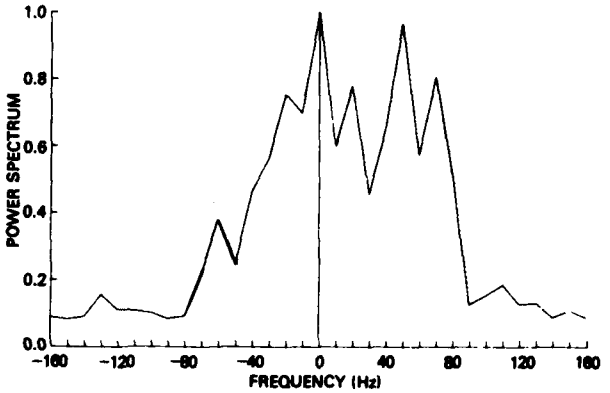

(c) Record 3

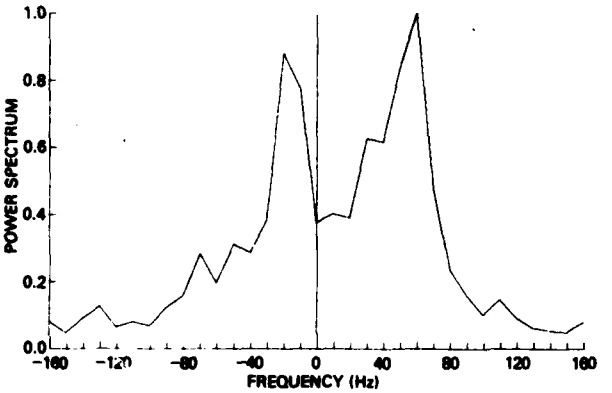

(d) Record 4

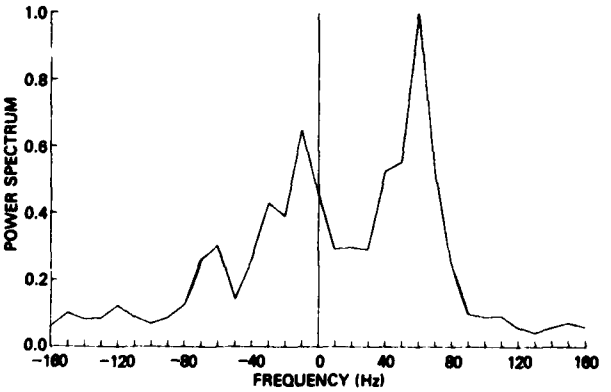

(e) Record 5

Fig. 5 — Doppler power spectra at 2.1 GHz. Each spectrum is the average of 17 32-point spectra. The data are from records 1 through 5 of range cell 3, file 6.

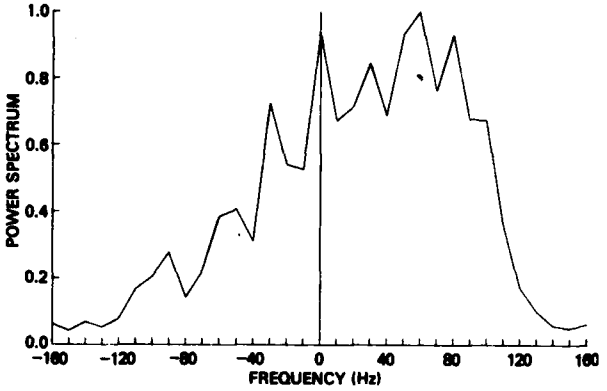

(a) Record 1

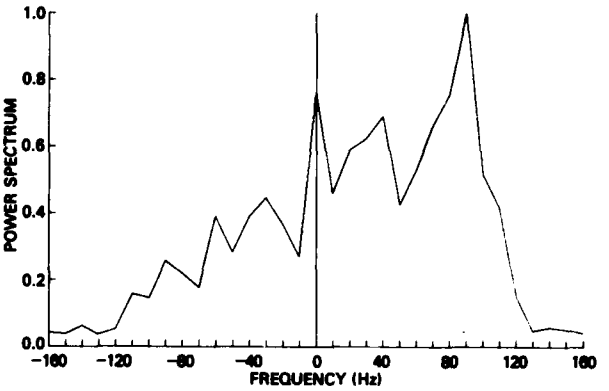

(b) Record 2

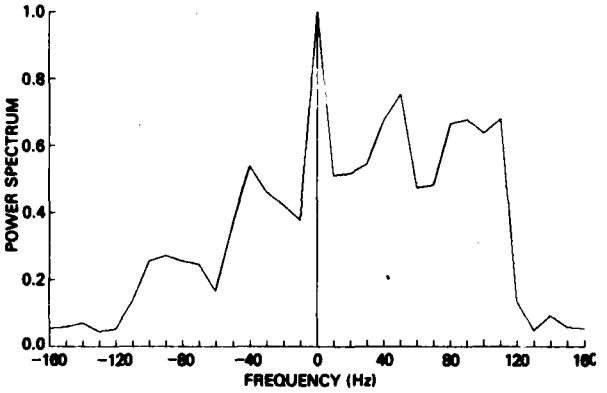

(c) Record 3

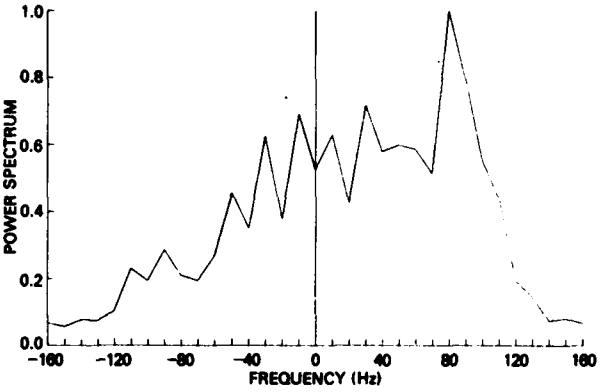

(d) Record 4

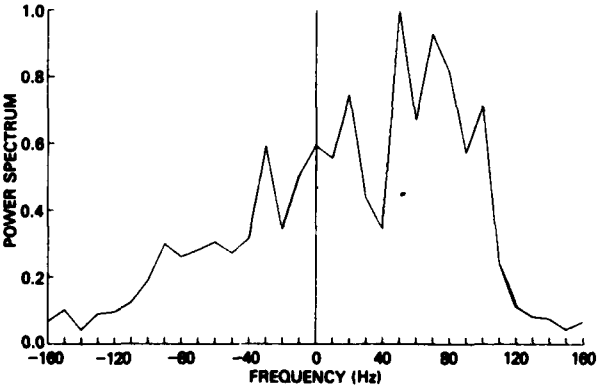

(e) Record 5

Fig. 6 — Doppler power spectra at 3.0 GHz. Each spectrum is the average of 17 32-point spectra. The data are from records 1 through 5 of range cell 3, file 6.

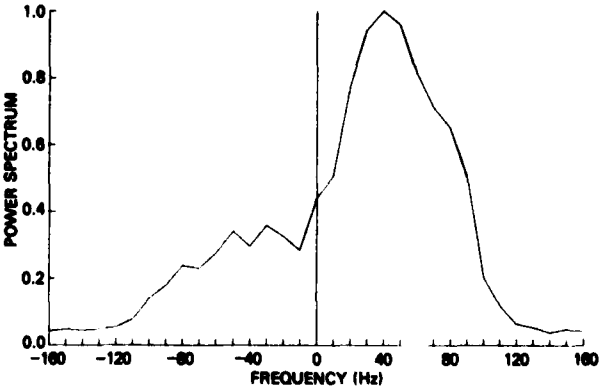

Fig. 7 — The "most typical" spectrum at 3.0 GHz, obtained by averaging records 1 through 5 in range cell 6

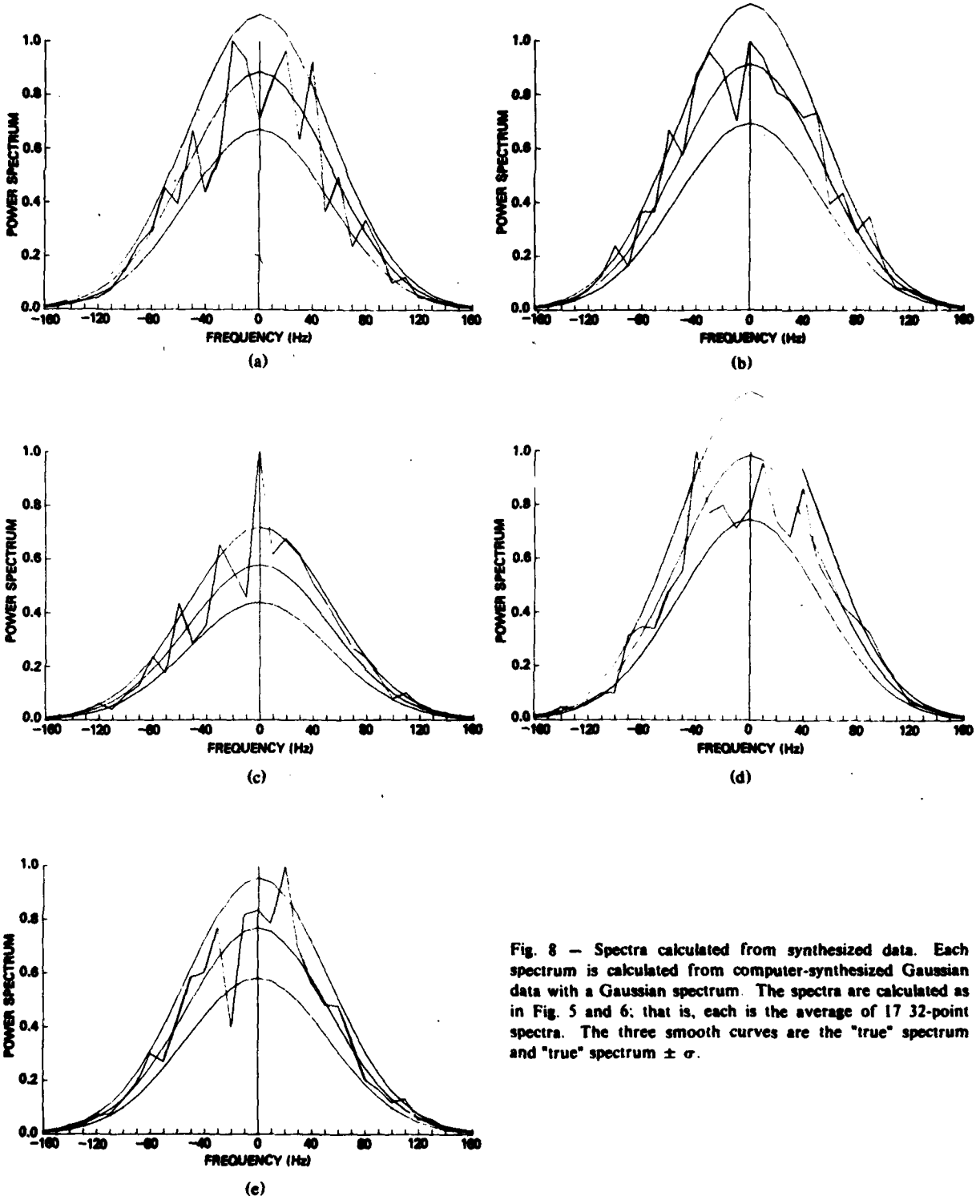

Fig. 8 — Spectra calculated from synthesized data. Each spectrum is calculated from computer-synthesized Gaussian data with a Gaussian spectrum. The spectra are calculated as in Fig. 5 and 6; that is, each is the average of 17 32-point spectra. The three smooth curves are the "true" spectrum and "true" spectrum $\pm \sigma$.

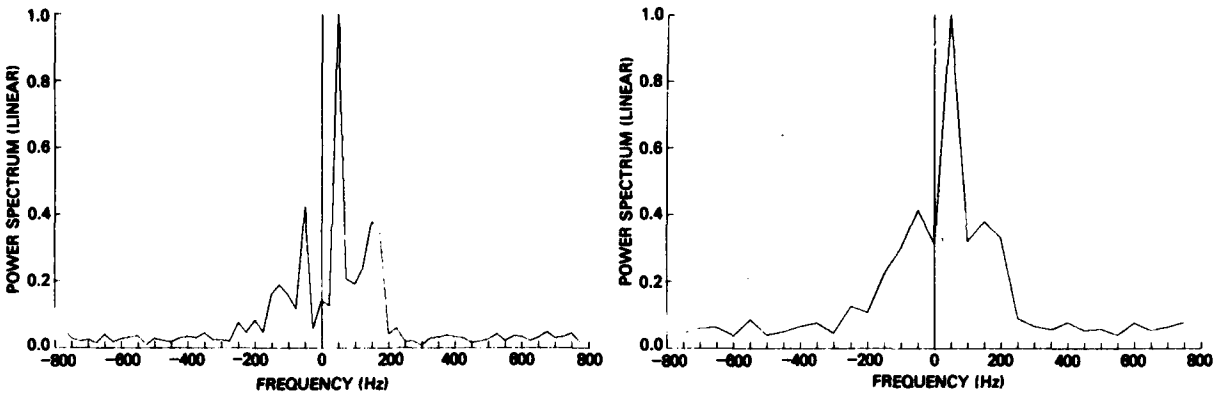

(a) Average of six 64-point spectra

(b) Average of 13 32-point spectra

Fig. 9 — Two typical spectra from file 3, the single-frequency file, with both spectra being calculated from the same data (from the same record and range cell). The antenna was rotating at 6 RPM.

Plots of spatial autocorrelation functions are shown in Fig. 12. These are computed as by Eq. (3), but in the present case the lags are spatial rather than temporal. The compressed pulse width of 0.7 μs corresponds to a resolution cell width of 105.0 m; however, as was mentioned, there is 50% overlap between successive range cells. Hence each spatial lag in these plots is equal to 52.5 m. The plots shown in Fig. 12 are smoothed values of ρ which were obtained by averaging the results of ten consecutive pulses.

The most commonly accepted model for the Doppler power spectrum is the Gaussian model, and the corresponding correlation function [1, p. 334] is a *damped* sinusoid of the form

$$\rho(t) = e^{-2(2\pi\sigma_v t/\lambda)^2} \cos(4\pi V_0 t/\lambda), \tag{4}$$

where V_0 is the mean velocity and σ_v is the RMS velocity of the clutter. According to Nathanson [1, p. 334] the value of $\rho(t)$ is not very dependent on the actual spectrum shape. However, the values we obtain for $\rho(t)$ are often much smaller than the theoretical values calculated according to Eq. (4) (with σ_v and V_0 computed from the data). This has serious implications for the predicted performance of MTI filters employing delay-line cancelers. For example, the clutter attenuation factors for single and double delay-line cancelers are

$$CA_1 = [1 - \rho(t)]^{-1}$$

and

$$CA_2 = [1 - (4/3)\rho(t) + (1/3)\rho(2t)]^{-1},$$

and, without pressing very hard, we have found that the difference between the theoretical and actual values of ρ can easily produce a corresponding difference of 5 dB for CA_1 and 10 dB for CA_2. For spectra having a variable number of peaks whose positions are also variable, it might be desirable to use an *adaptive* MTI to achieve clutter rejection.

SPATIAL, TEMPORAL, AND FREQUENCY VARIATION

Notation

Three types of averages appear in our subsequent discussion, indicated by boldface type, single bars, and double bars. To illustrate, we consider the three types of "mean power":

For each of the five frequencies f_i, $\mathbf{P}_i = \mathbf{P}_i(r, c)$ denotes the theoretically "true" or ensemble mean power which is characteristic of the return at the ith frequency from the rth record from the cth

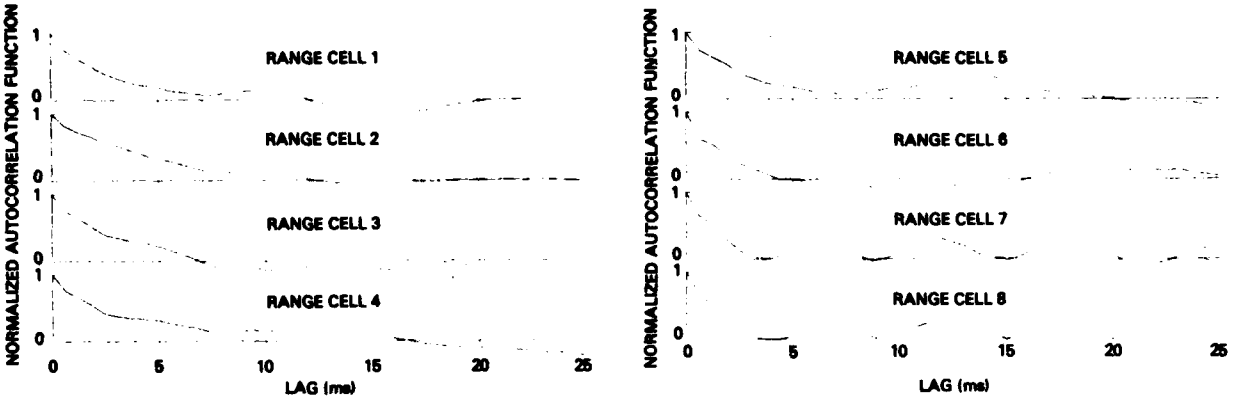

Fig. 10 — Temporal autocorrelation from file 3, the single-frequency file

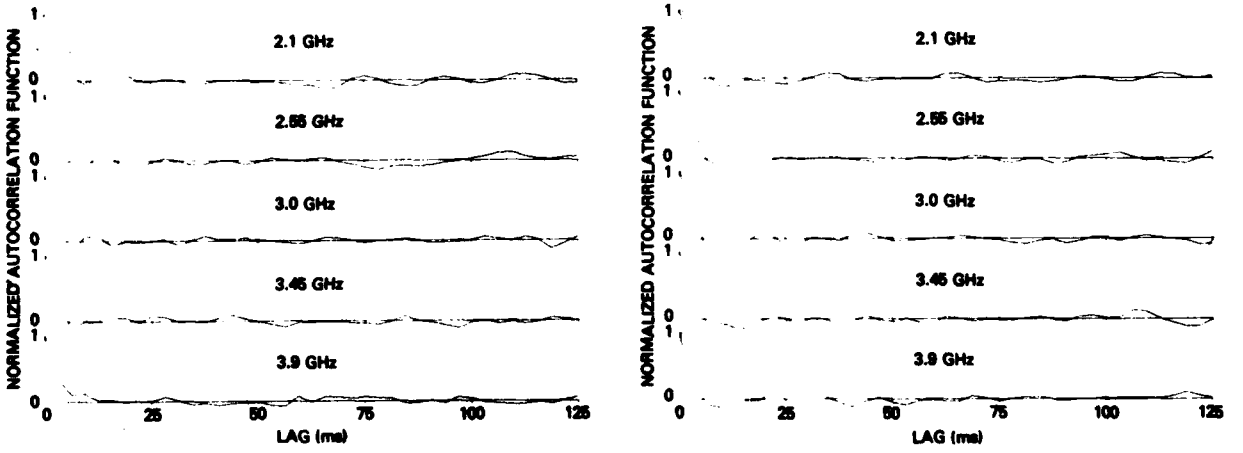

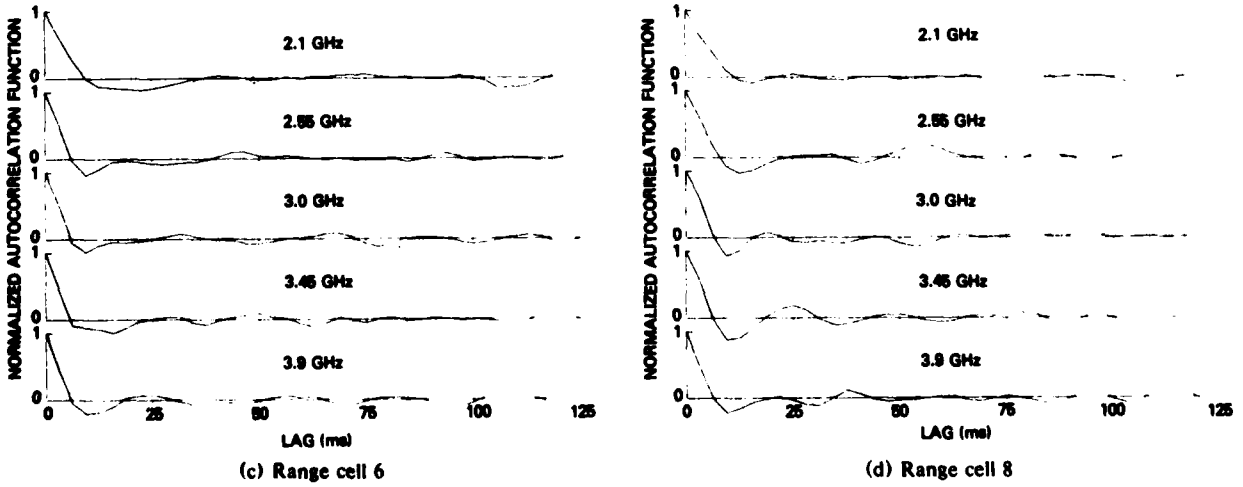

Fig. 11 — Temporal autocorrelation from file 6, a multifrequency file

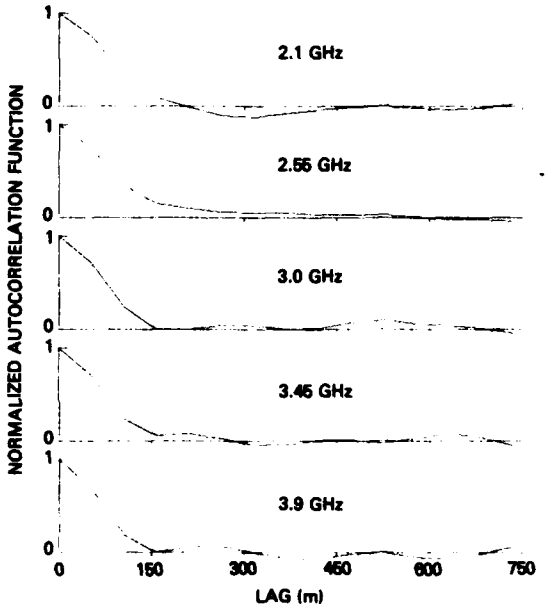

Fig. 12 — Spatial autocorrelations. The data are from file 1, and each correlogram is a ten-pulse average (pulses 1 through 10).

range cell. The sample mean $\bar{P}_i = \bar{P}_i(r, c)$ is the numerical average of the N values of instantaneous power contained in the rth record from the cth range cell, where $N = 85$ for files 1 and 2 and $N = 562$ for files 5 and 6. Similarly, $\bar{\bar{P}}_i$ denotes the numerical average of *all* the values of instantaneous power (all records from all range cells) contained in a given file. Thus, each file gives rise to $M_r \cdot M_c$ values $\bar{P}_i(r, c)$, where $1 \leqslant r \leqslant M_r$ and $1 \leqslant c \leqslant M_c$, but to only one value of $\bar{\bar{P}}_i$:

$$\bar{\bar{P}}_i = \frac{1}{M_r \cdot M_c} \sum_r \sum_c \bar{P}_i(r, c).$$

In theory one attempts to relate the quantities $\mathbf{P}_i$ to the physical properties of the clutter. In practice, the true means $\mathbf{P}_i$ are approximated by the sample means $\bar{P}_i$, and the experimental verification of any physical model is complicated by random statistical fluctuations in the quantities $\bar{P}_i$ which are due to the Gaussian nature of the voltages and would exist even in the absence of receiver noise.

In general, data from different files is never collated, and the above notation will be followed consistently. These general rules are violated only in the case of receiver noise. The quantities $\mathbf{N}_i$ are approximated by the file averages $\bar{\bar{N}}_i$ obtained from the noise file, and we shall use the same symbol $\mathbf{N}_i$ for both the true value and its estimate $\bar{\bar{N}}_i$. Thus, for example, we shall write $\bar{P}_i - \mathbf{N}_i$ instead of $\bar{P}_i - \bar{\bar{N}}_i$ for the "noise corrected" value of the indicated sample mean. In practice, the difference $|\mathbf{N}_i - \bar{\bar{N}}_i|$ is small, since each $\bar{\bar{N}}_i$ is the numerical average of 26,400 values of instantaneous noise power.

Nonhomogeneity of the Clutter

Figure 13 represents the spatial arrangement of rain based on the envelope-detected radar return. The data are from file 3, the single-frequency file. A standard lineprinter has been used to display the results. Each print line is one radar pulse, with each character position in the line representing a range cell. The data from each range cell of each pulse is quantized to a three-level scale, with the first level (blank) consisting of returns below 9, the second level (plus sign) consisting of returns between 9 and 20, and the third level (letter M) consisting of returns greater than 20. The data appear to contain various eddies. Since constant-false-alarm-rate (CFAR) detectors assume a homogeneous distribution in the detector reference cells, rain clutter will produce a larger number of false alarms than expected.

Fig. 13 — Spatial power plot of rain

Table 5 shows values of the record-averaged quantities $\bar{\bar{P}}_3 - \mathbf{N}_3$ tabulated against range cell, for each of the two records 4 and 5 in files 1 and 2. A sharp gradient can be perceived in the data from file 1. The standard deviation in $\bar{\bar{P}}_3 - \mathbf{N}_3$ produced by purely random fluctuations in these two files is generally of the order of $(0.1)\bar{\bar{P}}_3$, and the variation in $\bar{\bar{P}}_3 - \mathbf{N}_3$ from record to record and range cell to range cell is typically larger than this.

The Ideal Power-Versus-Frequency Relation

From a straightforward analysis of the effects of receiver noise and calibration errors, one obtains the relation

$$\mathbf{P}_i = Z_i \mathbf{F}(f_i) + \mathbf{N}_i, \tag{5}$$

where $\mathbf{F} = \mathbf{F}(f)$ is the "ideal" power-versus-frequency relation that would be observed in the absence of calibration errors and noise and Z_i is the calibration error at the ith frequency. Hence, $Z_i \equiv 1$ if the calibration is perfect, and $\mathbf{N}_i \equiv 0$ in the absence of noise. Our problem is to use the data $\bar{\bar{P}}_i$ to obtain information about the function $\mathbf{F} = \mathbf{F}(f)$, which depends on the radar range R as well as other parameters descriptive of the clutter.

Table 5 — Record-Averaged Noise-Corrected Power ($\bar{\bar{P}}_3 - N_3$)

Range Cell	Power			
	File 1		File 2	
	Record 4	Record 5	Record 4	Record 5
1	163.93	110.24	173.28	178.76
2	158.16	105.21	222.55	199.23
3	215.29	121.16	270.30	246.79
4	181.95	140.36	254.44	233.01
5	168.23	112.73	301.91	278.24
6	210.08	108.14	381.97	333.75
7	232.01	164.65	384.43	351.03
8	259.35	192.03	341.37	346.16
9	261.11	246.94	299.08	390.74
10	253.45	261.67	353.78	455.12
11	200.16	321.06	526.65	430.40
12	223.20	319.85	538.09	418.65
13	278.63	291.59	523.79	551.30
14	296.53	297.09	602.55	586.94
15	317.79	232.75	621.46	651.76
16	428.91	211.11	672.00	815.69
17	455.43	311.56	832.99	840.75
18	602.76	378.09	866.55	735.04
19	695.36	467.98	639.72	659.79
20	682.16	453.22	591.72	861.64
21	466.94	540.24	778.02	891.25
22	521.89	713.58	831.37	781.01
23	803.76	809.74	702.62	799.22
24	973.81	778.86	685.38	897.97
25	1068.90	989.52	792.05	838.75
26	1152.64	962.83	926.96	655.86
27	1100.74	796.81	746.35	492.04
28	1079.18	727.39	706.39	531.99
29	1017.65	795.35	831.69	498.71
30	1112.04	1245.36	822.87	467.36
31	1489.19	1367.94	695.41	446.66
32	1769.84	1193.32	555.47	460.21
33	1620.96	1052.68	416.80	466.17
34	1488.48	1140.50	391.64	438.13
35	1334.06	1526.23	371.10	362.48
36	1631.59	1629.15	344.59	351.86
37	1646.35	1275.93	367.83	389.25
38	1445.51	1189.55	348.08	369.44
39	1273.94	1122.02	346.94	390.45
40	1173.75	1302.71	443.90	349.97
41	1091.18	1554.43	504.90	383.08
42	1135.10	1538.92	470.01	402.79
43	1135.81	1378.86	341.11	410.01
44	1128.04	1393.89	382.57	353.60
45	1289.82	1583.34	384.74	289.66
46	1289.44	1632.78	325.75	300.09
47	1732.34	1445.54	414.50	347.80
48	2118.45	1314.08	411.51	332.99
49	1660.51	1263.01	348.02	379.02
50	1354.62	1188.23	365.67	361.28
51	1531.50	1234.49	344.20	312.34
52	1765.66	1438.20	297.53	322.77
53	1693.00	1626.90	299.35	358.48
54	1545.73	1459.48	243.01	443.04
55	1411.74	1478.97	296.14	446.76
56	1386.58	1617.51	430.98	400.71
57	1384.94	1645.16	420.86	401.76
58	1389.48	1402.46	481.95	317.12
59	1465.61	1300.81	481.75	283.85
60	1552.63	1389.47	373.71	250.32
61	1447.44	1237.25	349.18	315.91
62	1420.55	1167.37	306.37	324.04
63	1507.13	1072.47	365.45	330.07
64	1611.69	979.02	427.05	399.82

Table 6 shows the calibrated values of instantaneous power averaged over *all* the data in each file, that is, $\bar{\bar{P}}_i$. These data are tabulated only for the multifrequency files, including the noise file, file 8. The noise power is not flat across the frequency range because the calibration involved certain factors (such as antenna gain) which do not affect the receiver noise. Also the signal-to-noise ratios $\bar{\bar{P}}_i/N_i$ vary from file to file. File 5 is by far the noisiest file, the signal-to-noise ratios in this file all being less than 9 dB. The "relative values of noise-corrected power" are defined by

$$\bar{\bar{Q}}_i = (\bar{\bar{P}}_i - N_i)/(\bar{\bar{P}}_1 - N_1) \tag{6a}$$

and

$$\bar{Q}_i = (\bar{P}_i - N_i)/(\bar{P}_1 - N_1). \tag{6b}$$

The quantities $\bar{\bar{Q}}_i$ are tabulated in Table 7. As can be seen, the corresponding values of $\bar{\bar{Q}}_i$ are fairly constant from file to file. This suggests the model

$$P(f_i) = AQ(f_i) + N_i.$$

Table 6 — File-Averaged Values of Calibrated Power $\bar{\bar{P}}_i$

Frequency (Ghz)	Power $\bar{\bar{P}}_i$				
	File 1	File 2	File 5	File 6	File 8
2.1	141.5	77.5	14.9	39.7	6.3
2.55	451.2	244.9	42.5	127.9	12.9
3.0	889.5	480.6	64.1	268.5	12.6
3.45	1241.1	705.1	95.5	389.4	12.9
3.9	814.1	434.8	79.8	246.3	24.3

Table 7 — Relative Values of File-Averaged, Noise-Corrected Power $\bar{\bar{Q}}_i$

Frequency (GHz)	Power $\bar{\bar{Q}}_i$			
	File 1	File 2	File 5	File 6
2.1	1.00	1.00	1.00	1.00
2.55	3.24	3.26	3.44	3.44
3.0	6.49	6.57	5.99	7.66
3.45	9.08	9.72	9.61	11.27
3.9	5.84	5.76	6.45	6.64

where A is a frequency-independent parameter which varies from file to file and $Q = Q(f)$ is a function which depends on frequency *only* and no other parameters. However, for reasons mentioned in the Introduction, we are not very interested in the behavior of heavily averaged data. We therefore restrict our attention to data contained in a single file (or portion thereof), and we consider whether the data *within a given file* conforms to the model

$$\mathbf{P}_i = A\mathbf{Q}_i + \mathbf{N}_i, \tag{7}$$

where the parameter A varies with time and position but not with frequency whereas the function

$$\mathbf{Q}_i = \mathbf{Q}(f_i) = (\mathbf{P}_i - \mathbf{N}_i)/(\mathbf{P}_1 - \mathbf{N}_1) \tag{8}$$

depends only on frequency. Comparing Eq. (7) to Eq. (5), we see that the model given by Eq. (7) asserts that the "ideal" mean-power-versus-frequency relation is

$$\mathbf{F}(f_i) = A \cdot (\mathbf{Q}_i/Z_i), \tag{9}$$

where the first factor contains all the spatial and temporal dependence and the second factor contains all the frequency dependence.

Parenthetically, the validity of the model given by Eq. (7) was somewhat unexpected. In the literature one finds discussions of various scattering mechanisms (discussed in the next subsection), each of which give rise to an ideal law of the type $\mathbf{P} = Af^n$ (in the absence of noise and calibration errors), with different effects giving rise to different values of n. If, say, two such effects are operating simultaneously, then

$$\mathbf{P}_i = A_1 f^m + A_2 f^n + \mathbf{N}_i,$$

which does not conform to Eq. (7), since the noise-independent part cannot be expressed as the product $A \cdot Q(f)$, where A is frequency independent. Before examining the data, we expected to observe a law of this type with $m = 4$ and $0 \leqslant n \leqslant 2$. Physically this corresponds to certain turbulence effects superimposed upon a more-or-less uniform distribution of clutter in the beam.

Again, $\mathbf{P}_i = \mathbf{P}_i(r, c)$ varies with record r and range cell c, and the hypothesis now to be tested is that, for data within a given file, $\mathbf{Q}_i$ does *not* vary with r and c. The quantities $\mathbf{Q}_i$ are approximated by the quantities $\bar{Q}_i$, and to test the hypothesis, the standard deviations of the $\bar{Q}_i$ are first calculated theoretically, *on the assumption* that the $\mathbf{Q}_i$ are constant. Then these theoretically calculated standard deviations are compared with the actual sample standard deviations computed directly from the $M_r \cdot M_c$ samples of $\bar{Q}_i$ contained in the given file. The results are shown in Table 8. In our theoretical calculations we neglected the effects of receiver noise, which explains why the agreement is not as good in the noisy files 5 and 6 as in files 1 and 2. Keeping in mind the nature and effects of these simplifying assumptions, we judge that the results presented in Table 8 represents good fit between the data and the model. Details of the statistical analyses are given in Ref. 4. The validity of this result is not affected by the presence of the calibration errors Z_i, since they are constants and their effects are multiplicative. In fact it can be shown [4] that ratios of the calculated to the sample standard deviations shown in Table 8 are mathematically identical to the values that are obtained by using the raw uncalibrated data.

Table 8 — Comparison of Theoretically Calculated Standard Deviations of $\bar{Q}_i$ with Sample Standard Deviations of $\bar{Q}_i$

	Standard Deviation											
	File 1			File 2			File 5			File 6		
Frequency (GHz)	Sample	Theo-retical	Ratio	Sample	Theo-retical	Ratio	Sample	Theo-retical	Ratio	Sample	Theo-retical	Ratio
2.1	—	—	—	—	—	—	—	—	—	—	—	—
2.55	1.00	0.90	1.11	0.86	0.87	0.99	0.75	0.44	1.70	0.31	0.26	1.21
3.0	1.86	1.82	1.02	1.94	1.92	1.01	0.96	0.78	1.22	0.71	0.58	1.22
3.45	2.49	2.52	0.99	2.71	2.78	0.98	1.65	1.29	1.28	0.95	0.82	1.16
3.9	1.70	1.64	1.04	1.57	1.67	0.94	1.02	.83	1.23	0.62	0.48	1.29

Evidence for the Vertical-Stratification Model

As mentioned in the Introduction, two physical mechanisms could explain the existence of multiple peaks in the clutter Doppler spectra: wind shear operating on a vertically stratified medium, and Bragg-type scattering from turbulent eddies. We will now briefly describe why we believe the data favor the vertical stratification model. Details of the analysis, which is rather prolix, are given in Ref. 5.

We have shown that the data within any given file is consistent with the operation of a simple power-versus-frequency relation (Eq. (9)) involving only a single multiplicative, frequency-independent, and variable parameter A. For a perfectly calibrated system the power-versus-frequency law given by Eq. (9) assumes the form

$$\mathbf{F}(f) = A \cdot \mathbf{Q}(f), \tag{10}$$

where, again, the function $\mathbf{Q}$ contains all of the frequency dependence. The simplest law of this kind is given by

$$\mathbf{F}(f) = A \cdot f^n, \tag{11}$$

where the exponent n is fixed. In the literature one finds discussions of various scattering mechanisms, each of which give rise to an ideal power-versus-frequency law of this type. For the classical case of incoherent scattering from drops uniformly distributed throughout the radar resolution cell, we have $n = 4$ [5]. For incoherent scattering from narrow horizontal bands or clumps of clutter, it turns out that $n = 5$ [4], whereas the Bragg-scattering effects discussed in the literature are expected to produce

values of n which lie in the range $0 \leqslant n \leqslant 2$ [6-8]. (In addition, certain coherent scattering effects discussed by Kerr [3] would also produce exponents in the range $0 \leqslant n \leqslant 2$.) In all these theoretical formulations, it is assumed that the radar cross section σ of each drop follows the Rayleigh scattering law, $\sigma \propto f^4$, and due account is taken of the variation of the size of the radar resolution cell with frequency.

The object of our analysis is to decide between the two alternative models: Bragg scattering ($0 \leqslant n \leqslant 2$), and vertical stratification of the clutter ($n = 5$). From the data in each record from each range cell, we formed four estimates of n according to

$$\hat{n}_M = \sum_{i=1}^{M} \xi_i^{(M)} \log (\bar{P}_i - \mathrm{N}_i), \tag{12}$$

for $M = 2$, 3, 4, and 5; that is, we formed each estimate $\hat{n}_M$ by using only the first M frequencies. We chose the weights $\xi_i^{(M)}$ so that Eq. (12) gives the correct result ($\hat{n}_M = n$) in the absence of calibration errors and receiver noise, and among all such estimates we chose the one which minimizes the effects of calibration errors (since the effects of receiver noise are smaller and can be averaged out). It turns out that these "optimal" weights are given by

$$\xi_i^{(M)} = \left[\log f_i - \frac{1}{M} \sum_{j=1}^{M} \log f_j\right] \cdot \left[\sum_{j=1}^{M} (\log f_j)^2 - \frac{1}{M} \left(\sum_{j=1}^{M} \log f_j\right)^2\right]^{-1} \tag{13}$$

Each data file gives rise to $M_r \cdot M_c$ values of $\hat{n}_M$ (one from each record from each range cell). The file-averaged quantities $\bar{\hat{n}}_M$ are shown in Table 9. For each fixed M the file-to-file variation of $\bar{\hat{n}}_M$ is rather small, but within each given file the variation $\bar{\hat{n}}_M$ with M is rather large and systematic. The sample standard deviations in $\hat{n}_M$ are shown in Table 10. The values of these quantities fall within the range of statistical expectation on the assumption that the ideal power-versus-frequency law is given by $F(f) = Af^n$, where A is frequency independent.

Table 9 — Values of Exponent Estimates $\bar{\hat{n}}_M$

File	$\bar{\hat{n}}_2$	$\bar{\hat{n}}_3$	$\bar{\hat{n}}_4$	$\bar{\hat{n}}_5$
1	6.0	5.2	4.5	3.1
2	6.2	5.4	4.6	3.2
5	5.8	4.6	4.2	3.0
6	6.3	5.7	4.9	3.4

Table 10 — Sample Standard Deviations of $\hat{n}_M$

File	$SD(\hat{n}_2)$	$SD(\hat{n}_3)$	$SD(\hat{n}_4)$	$SD(\hat{n}_5)$
1	1.33	0.74	0.49	0.37
2	1.15	0.68	0.47	0.34
5	0.79	0.45	0.41	0.26
6	0.38	0.25	0.18	0.13

We now come to the heart of our analysis. It can be shown that the effects of receiver noise on $\bar{\hat{n}}_M$ are small and that the errors $\bar{\hat{n}}_M - n$ are almost entirely due to the calibration errors Z_i:

$$\bar{\hat{n}}_M = n + \sum_{i=1}^{M} \xi_i^{(M)} \log Z_i.$$

The second term on the right-hand side has the form of a vector dot product between the vectors $\{\xi_i^{(M)}\}$ and $\{\log Z_i\}$, and using a certain generalization of the Schwarz inequality, one can obtain lower bounds to the RMS calibration errors (dB),

$$\text{RMS} = \left[\frac{1}{M}\sum_{i=1}^{M}(10\log_{10} Z_i)^2\right]^{1/2}, \tag{14}$$

in terms of the quantities $\bar{\bar{n}}_M - n$. These lower bounds are shown in Table 11, with the data being from file 6. In this table the assumed "true" value of n is increased in integral steps from $n = 0$ to $n = 10$, and each entry shows a lower bound to the RMS calibration errors (dB) defined by Eq. (14). An RMS value above 2 dB is considered to be beyond the range of credibility, and it is on this basis that we reject the Bragg-scattering model, since values of n in the range $0 \leqslant n \leqslant 2$ would imply RMS calibration errors of 3 dB and more. Also, the smallest lower bounds are obtained near $n = 5$, which corresponds to vertical stratification (scattering from narrow horizontal bands of dense clutter). Finally, the evidence is especially compelling if we exclude the line at $M = 5$, which contains the results involving the anomaly at the highest frequency (3.9 GHz).

Table 11 — Lower Bounds to the RMS Calibration Error $\left(= \left[\frac{1}{M}\sum_{1}^{M}(10\log_{10} Z_i)^2\right]^{1/2}\right)$ for Assumed Exponents n. The data are from file 6.

M	Lower Bound (dB)										
	n=0	n=1	n=2	n=3	n=4	n=5	n=6	n=7	n=8	n=9	n=10
2	2.7	2.2	1.8	1.4	1.0	0.6	0.1	0.3	0.7	1.1	1.6
3	4.4	3.7	2.9	2.1	1.4	0.6	0.4	1.1	1.8	2.6	3.4
4	5.6	4.5	3.4	2.3	1.2	0.7	1.4	2.5	3.6	4.7	5.8
5	5.3	3.8	2.5	2.0	2.1	2.7	4.1	5.6	7.0	8.5	10.0

SUMMARY OF THE MAIN CONCLUSIONS

The conclusions to be listed are not intended to represent general facts which hold in every case, and one would expect that measurements taken under different meteorological conditions could yield different results. Moreover, besides these conclusions themselves it is of equal importance to emphasize the nature of the statistical methods used to obtain them, which were designed to be valid in the presence of calibration errors and without the assumption that the clutter process was stationary (homogeneous) over extended regions of space or durations of time. In particular, we did not attempt to establish trends or functional relationships by "fitting curves" to the data. Even in the absence of calibration errors, such regression techniques could establish only the "average" behavior of the clutter, which would be of little use either in gaining an understanding of the rapidly changing clutter process or in designing radar systems which must work in a highly variable and complex environment. For example, the heavily averaged spectrum shown in Fig. 7 indicates the presence of a wind shear but gives no hint to the vertical stratification suggested by the spikiness of some of the spectra shown in Fig. 5.

Of the four points of summary that follow, the first two (which are purely empirical) have potentially serious implications for the performance of CFAR and MTI detectors, and the last two are concerned with determining what physical mechanisms might be involved in the production of multipeaked clutter spectra:

- The clutter was nonhomogeneous in space and nonstationary in time. Large qualitative differences could sometimes be discerned in clutter spectra which were as little as 2 s apart (which was the smallest elapsed time between consecutive data records).

- The clutter Doppler spectra were non-Gaussian in shape, and the spectra were frequently multipeaked. Although the radar was looking into the wind at the surface, every single spectrum showed a significant amount of signal energy in the negative Doppler range, indicating the presence of a wind shear.

- An analysis of the variation of backscattered power with position, time, and frequency revealed that the data were consistent with the operation of a simple ideal mean-power-versus-frequency relation of the type $P = A \cdot Q(f)$, where A is a frequency-independent parameter which varies with time and position and $Q = Q(f)$ is some function which depends *only* on frequency. (This result is valid in the presence of calibration errors and could even have been obtained from the raw uncalibrated data.)

- The multiple peaks which were observed in the clutter spectra could have been caused by the wind shear operating on a vertically stratified medium or by Bragg scattering from turbulent eddies. For Bragg scattering, $Q(f) = f^n$, where n falls in the range $0 \leqslant n \leqslant 2$, whereas scattering from horizontal bands or clumps of clutter would produce the exponential value $n = 5$. To establish a reasonable range of exponential values, lower bounds to the RMS calibration errors were calculated in terms of the quantities $\hat{n} - n$, where n is an assumed "true" value (varied from 0 to 10 in integral steps) and $\hat{n}$ is its estimate (formed from certain weighted logarithmic sums). Values of n which implied RMS calibration errors larger than 2 dB were rejected as reasonable possibilities, and on this basis the vertical-stratification model ($n = 5$) is favored over the Bragg-scattering model ($0 \leqslant n \leqslant 2$), since the latter implies RMS calibration errors larger than 3 dB. In fact, the "reasonable" range of exponential values was found to lie in the interval $3 < n < 7$, and the smallest lower bounds to the RMS calibration error occurred at values of n close to 5.

ACKNOWLEDGMENT

The authors gratefully acknowledge the help of George J. Linde, who collected the data, calibrated the system, and very patiently explained its operations.

REFERENCES

1. F.E. Nathanson, *Radar Design Principles*, McGraw-Hill, New York, 1969.

2. E.J. Barlow, "Doppler radar," Proc. IRE **37**, 340-355 (1949).

3. D.E. Kerr, *Propagation of Short Radio Waves*, M.I.T. Radiation Lab, Series 13, McGraw-Hill, New York, 1951.

4. W.B. Gordon, "Analysis of rain clutter data from a frequency agile radar," Radio Science **17**, 801-816 (1982).

5. M.I. Skolnik, *Introduction to Radar Systems*, McGraw-Hill, New York, 1962.

6. E.E. Gossard, "A fresh look at the radar reflectivity of clouds," Radio Sci. **14**(5), 1089-1097 (1979).

7. E.E. Gossard and R.G. Strauch, "The internal radio refractive index spectra of clouds from UHF forward scatter radar observations," pp. 704-707 in *Proceedings, 19th Conference on Radar Meteorology*, Am. Met. Soc., Apr. 1980.

8. K. Naito and D. Atlas, "On microwave scatter by partially coherent clouds," pp. 7-12 in *Proceedings, 12th Conference on Radar Meteorology*, Am. Met. Soc., 1966.

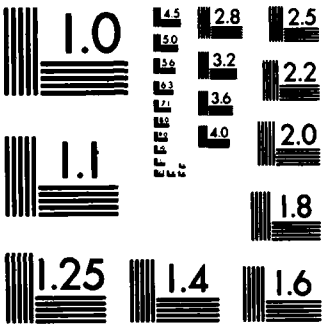

MICROCOPY RESOLUTION TEST CHART
NATIONAL BUREAU OF STANDARDS-1963-A